

# Compact wavelength de-multiplexer design using slow light regime of photonic crystal waveguides

Ahmet E. Akosman,<sup>1,\*</sup> Mehmet Mutlu,<sup>1</sup> Hamza Kurt,<sup>2</sup> and Ekmel Ozbay<sup>1</sup>

<sup>1</sup>Department of Electrical and Electronics Engineering, Nanotechnology Research Center, Bilkent University, 06800 Ankara, Turkey

<sup>2</sup>Department of Electrical and Electronics Engineering, TOBB University of Economics and Technology, 06560 Ankara, Turkey

\*akosman@ee.bilkent.edu.tr

**Abstract:** We demonstrate the operation of a compact wavelength de-multiplexer using cascaded single-mode photonic crystal waveguides utilizing the slow light regime. By altering the dielectric filling factors of each waveguide segment, we numerically and experimentally show that different frequencies are separated at different locations along the waveguide. In other words, the beams of different wavelengths are spatially dropped along the transverse to the propagation direction. We numerically verified the spatial shifts of certain wavelengths by using the two-dimensional finite-difference time-domain method. The presented design can be extended to de-multiplex more wavelengths by concatenating additional photonic crystal waveguides with different filling factors.

©2011 Optical Society of America

**OCIS codes:** (050.0050) Diffraction and gratings; (050.5298) Photonic crystals; (060.1810) Buffers, couplers, routers, switches, and multiplexers.

---

## References and links

1. J. E. Centeno, B. Guizal, and D. Felbacq, "Multiplexing and demultiplexing with photonic crystals," *J. Opt. A, Pure Appl. Opt.* **1**(5), L10–L13 (1999).
2. M. Koshiba, "Wavelength division multiplexing and demultiplexing with photonic crystal waveguide couplers," *J. Lightwave Technol.* **19**(12), 1970–1975 (2001).
3. A. Sharkawy, S. Shi, and D. W. Prather, "Multichannel wavelength division multiplexing with photonic crystals," *Appl. Opt.* **40**(14), 2247–2252 (2001).
4. M. Notomi, A. Shinya, S. Mitsugi, E. Kuramochi, and H. Y. Ryu, "Waveguides, resonators and their coupled elements in photonic crystal slabs," *Opt. Express* **12**(8), 1551–1561 (2004).
5. F. Van Laere, T. Stomeo, C. Cambournac, M. Ayre, R. Brenot, H. Benisty, G. Roelkens, T. F. Krauss, D. Van Thourhout, and R. Baets, "Nanophotonic polarization diversity demultiplexer chip," *J. Lightwave Technol.* **27**(4), 417–425 (2009).
6. B. E. Nelson, M. Gerken, D. A. B. Miller, R. Piestun, C. C. Lin, and J. S. Harris, "Use of a dielectric stack as a one-dimensional photonic crystal for wavelength demultiplexing by beam shifting," *Opt. Lett.* **25**(20), 1502–1504 (2000).
7. S. Kamei, K. Iemura, A. Kaneko, Y. Inoue, T. Shibata, H. Takahashi, and A. Sugita, "1.5%- $\Delta$  athermal arrayed-waveguide grating multi/demultiplexer with very low loss groove design," *IEEE Photon. Technol. Lett.* **17**(3), 588–590 (2005).
8. M. Thorhauge, L. H. Frandsen, and P. I. Borel, "Efficient photonic crystal directional couplers," *Opt. Lett.* **28**(17), 1525–1527 (2003).
9. M. Bayindir and E. Ozbay, "Band-dropping via coupled photonic crystal waveguides," *Opt. Express* **10**(22), 1279–1284 (2002).
10. S. Boscolo, M. Midrio, and C. G. Someda, "Coupling and decoupling of electromagnetic waves in parallel 2D photonic crystal waveguides," *IEEE J. Quantum Electron.* **38**(1), 47–53 (2002).
11. T. Niemi, L. H. Frandsen, K. K. Hede, A. Harpoth, P. I. Borel, and M. Kristensen, "Wavelength-division demultiplexing using photonic crystal waveguides," *IEEE Photon. Technol. Lett.* **18**(1), 226–228 (2006).
12. A. Rostami, F. Nazaria, H. Alipour Banaei, and A. Bahrami, "A novel proposal for DWDM demultiplexer design using modified-T photonic crystal structure," *Photonics Nanostruct. Fundam. Appl.* **8**(1), 14–22 (2010).
13. Y. Tanaka, T. Asano, Y. Akahane, B.-S. Song, and S. Noda, "Theoretical investigation of a two-dimensional photonic crystal slab with truncated cone air holes," *Appl. Phys. Lett.* **82**(11), 1661–1663 (2003).
14. B.-S. Song, S. Noda, and T. Asano, "Photonic devices based on in-plane hetero photonic crystals," *Science* **300**(5625), 1537 (2003).
15. S. Fan, P. R. Villeneuve, J. D. Joannopoulos, and H. A. Haus, "Channel drop filters in photonic crystals," *Opt. Express* **3**(1), 4–11 (1998).

16. E. Viasnoff-Schwoob, C. Weisbuch, H. Benisty, C. Cuisin, E. Derouin, O. Drisse, G.-H. Duan, L. Legouézigou, O. Legouézigou, F. Pommereau, S. Golka, H. Heidrich, H. J. Hensel, and K. Janiak, "Compact wavelength monitoring by lateral outcoupling in wedged photonic crystal multimode waveguides," *Appl. Phys. Lett.* **86**(10), 101107 (2005).
17. L. Martinelli, H. Benisty, O. Khayam, G. H. Duan, H. Heidrich, and K. Janiak, "Analysis and optimization of compact demultiplexer monitor based on photonic crystal waveguide," *J. Lightwave Technol.* **25**(9), 2385–2394 (2007).
18. H. Benisty, C. Cambournac, F. Van Laere, and D. Van Thourhout, "Photonic-Crystal Demultiplexer With Improved Crosstalk by Second-Order Cavity Filtering," *J. Lightwave Technol.* **28**(8), 1201–1208 (2010).
19. H. J. Kim, I. Park, B. H. O, S. G. Park, H. Lee, and S. G. Lee, "Self-imaging phenomena in multi-mode photonic crystal line-defect waveguides: application to wavelength de-multiplexing," *Opt. Express* **12**(23), 5625–5633 (2004).
20. N. Shahid, M. Amin, S. Naureen, M. Swillo, and S. Anand, "Junction-type photonic crystal waveguides for notch- and pass-band filtering," *Opt. Express* **19**(21), 21074–21080 (2011).
21. F. S.-S. Chien, Y.-J. Hsu, W.-F. Hsieh, and S.-C. Cheng, "Dual wavelength demultiplexing by coupling and decoupling of photonic crystal waveguides," *Opt. Express* **12**(6), 1119–1125 (2004).
22. L. Wu, M. Mazilu, T. Karle, and T. F. Krauss, "Superprism phenomena in planar photonic crystals," *IEEE J. Quantum Electron.* **38**(4), 915–917 (2002).
23. A. Adibi, R. K. Lee, Y. Xu, A. Yariv, and A. Scherer, "Design of photonic crystal optical waveguides with singlemode propagation in the photonic bandgap," *Electron. Lett.* **36**(16), 1376–1378 (2000).
24. A. Taflove, *Computational Electrodynamics—The Finite-Difference Time-Domain Method*, (Artech House, Norwood, MA 2000).
25. J. P. Berenger, "A perfectly matched layer for the absorption of electromagnetic waves," *J. Comput. Phys.* **114**(2), 185–200 (1994).

## 1. Introduction

Photonic crystals (PCs) are strongly wavelength sensitive, high-index contrast dielectric materials. This sensitivity originates from the dispersive properties of the PC structure as a result of the wavelength scale refractive index modulation with certain crystal symmetry. The wavelength selectivity can be used for the benefit of designing compact optical filters, which are the key components of the wavelength division multiplexing (WDM) systems in optical communications [1–3]. De-multiplexers (DEMUX) with compact, cost-effective, polarization independent, low cross-talk and high spectral resolution are demanded for the optical communication systems [4, 5]. The common methods to achieve WDM operation using planar light wave circuits are based on thin-film filters, Bragg grating filters (high number of periods are required and large side lobes accompany the spectral response) and arrayed waveguide gratings (AWG) [6, 7]. Even though high spectral resolution and low cross-talk have been achieved using these methods, compactness and cost-effectiveness are still questionable [8]. One of the unique properties of the PCs is their extremely small footprints along with the rich dispersion characteristics [9]. Hence, we can claim that PC based DEMUX designs can be good candidates for implementing compact and effective wavelength monitoring for various applications including communications and sensing.

There have recently been various techniques studied by exploiting the different aspects of the wavelength selectivity features of PCs. For example, PC waveguide (PCW) directional couplers employing two parallel waveguides have been proposed and investigated for wavelength selectivity [8–10]. In all these studies, coupled waveguides are used to create the de-multiplexing mechanism by manipulating the waveguides. Different perturbations in the waveguide branches result in different resonance frequencies. In Ref. 10, the evanescent coupling occurs among the coupled waveguides. A rather different approach can be adapted such that the cutoff frequency of the PCW mode can be changed by structural modifications, for example by changing the radii of the border holes. This principle was used in Refs. 11 and 12 to selectively drop different wavelengths along the PCW. Micro-cavities are highly frequency selective structures and the resonance frequency of the cavity mode can be tuned to a different wavelength by modifying the size of the cavity. The different frequencies propagating along the waveguide can be selected by these cavities which are placed at the sides of the waveguide-centerline [13–15].

Broad enough PCWs that operate in the multi-mode regime have been studied for coarse wavelength de-multiplexing [16–20]. The fundamental mode and higher order mode interaction creates mini-stop-band (MSB) in the dispersion diagram where the higher order

mode has a lower group velocity which can be considered as slow light regime. As a result the higher order mode with the larger field penetration depth will be dropped from the main channel if one side of the waveguide wall is thinned. The locations of these MSBs can be adjusted by changing the widths of the waveguides. Consequently, different wavelengths can be selected at different propagation distances. In addition, the two-channel wavelength de-multiplexer structure based on the self-imaging phenomenon using a multi-mode PCW has been studied [21]. Finally, purely periodic PCs may show a strong wavelength discrepancy that can also be exploited for the purpose of designing a DEMUX. This principle has been implemented in Refs. 21 and 22. By further exploiting the super-prism effect along with the two features of PCs, i.e., negative refraction and negative diffraction, a four-channel optical de-multiplexer was demonstrated in Refs. 22 and 23.

The disadvantages of these early proposed DEMUX solutions such as occupying large areas or utilizing complex operation principles can be partially avoided by allowing PCW to operate at the close proximity of the slow light region.

## **2. Proposed wavelength selective structure**

In this study, we report a wavelength de-multiplexer design taking the benefit of the slow light phenomena in PCWs. The goal of this study is not implementing a DEMUX design that fulfills all of the aforementioned properties. Instead, we firstly plan to prove the operation mechanism of a DEMUX design employing a rather simple system with three channels. The proposed DEMUX is designed and optimized for single wavelength operation. The principle of the frequency selection mechanism is based on the modulation of the photonic band gap (PBG) confinement by altering the dielectric filling factors and electric-field distributions in the slow light regime. Each PCW section has a different filling factor that in turn produces different PBG regions. The PBG is the only confinement mechanism in the square-lattice dielectric PCW, because index based confinement does not occur. In PCWs, if the frequency of the propagating field is outside the PBG of the waveguide, then there is not any mechanism that supports the guiding of the light. As a result, the light starts to leak out of the waveguide. Depending on the number of wavelengths that we wish to perform de-multiplexing on, the number of the cascaded waveguides can be increased.

The critical part of the design benefits from the electromagnetic wave behavior in the vicinity of the slow light region. Figure 1(a) shows the light propagation through a single mode PCW. The strong confinement and propagating nature of the light can be observed using the steady-state field distribution. On the other hand, if the frequency of light is in the vicinity of the slow light region, the spatial distribution of light changes. The oscillation period along the longitudinal direction increases and the field penetrates deeper toward the transverse plane to the propagation direction. As a consequence, the interaction with the PC structure is increased. If the width of the PC is decreased on one side and coupled to a new PCW channel such that the evanescent field can leak out at the channel location, the wavelength selectivity can be achieved. The different wavelengths enter different slow light regimes if the filling factor of the PC section is altered.

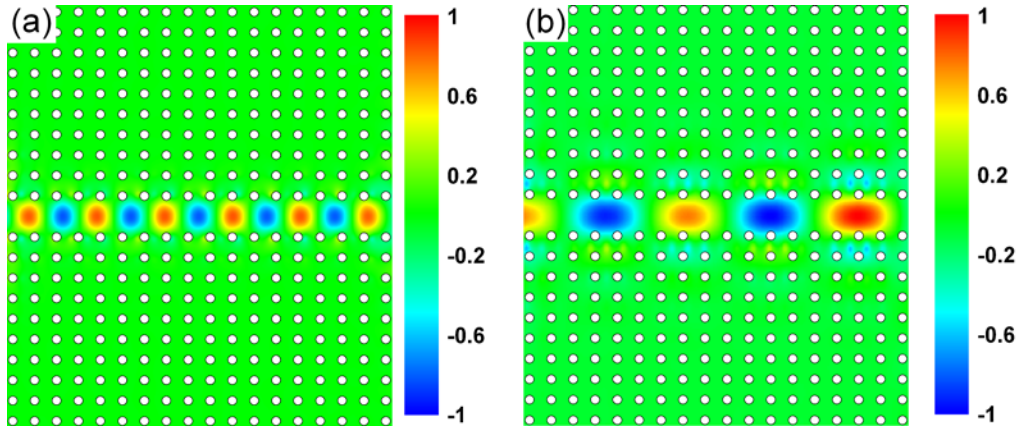


Fig. 1. (a) The steady-state electric field distribution when the wavelength of incident light corresponds to a propagating mode within the photonic crystal waveguide. (b) The field distribution for a different frequency, which is in the vicinity of the slow light regime. The same PCW is used in both cases.

Figure 2 shows the geometry of the proposed PCW device for the DEMUX design. It consists of three cascaded waveguides for which the dielectric filling factors are varied. The interface of each waveguide segment is indicated by a solid line. The waveguide is created as a result of removing one row of dielectric rods along the  $\Gamma X$  symmetry direction. The wavelength selectivity of the waveguides comes from the PBG effect and the slow light phenomenon as mentioned previously.

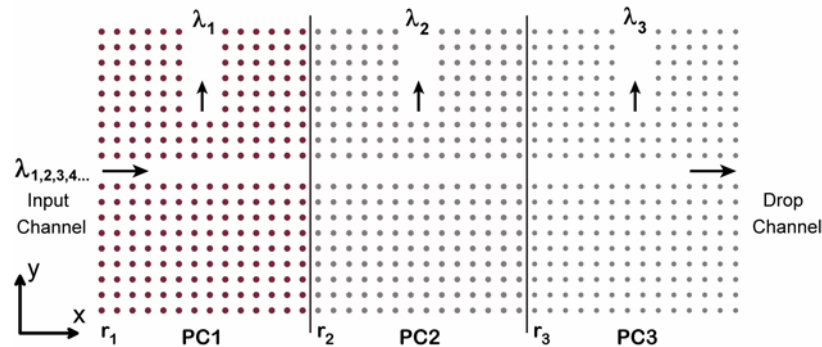


Fig. 2. The schematic of the device that is designed for the wavelength de-multiplexing. The different wavelengths are spatially separated at different locations along the  $x$ -direction. The complete structure is composed of three PCWs of different dielectric filling factors.

The finite-difference time-domain (FDTD) method is utilized for investigating the evolution of the different wavelengths that propagate through the concatenated PCWs [24]. The perfectly matched layer absorbing boundary condition surrounds the computational domain [25]. The unit-cell lattice  $a$  is discretized by 32 grid points. The input pulse is a modulated Gaussian pulse whose center frequency is varied to excite different channels. The incident wave is set to TM polarization (i.e., the electric field component is perpendicular to the propagation plane) to create a PBG region and a highly confined waveguide mode.

The complete structure consists of three sections and each section performs a testing by checking the wavelength of the incoming pulse. The parameters of each section are selected by investigating the cut-off frequencies of the waveguide bands of the PCW structures as shown in Fig. 3. The first PCW has the highest dielectric filling factor with,  $f = 15.2\%$  and the radius of the rods is  $r_1 = 0.22a$  (point C in Fig. 3). The filling factors of the second and the

third section are decreased to 12.57% and 10.18%, respectively, by setting  $r_2 = 0.20a$  and  $r_3 = 0.18a$  (points B and A, respectively). As a result of decreasing the filling factors, the frequency of the slow light regime increases as shown in Fig. 4.

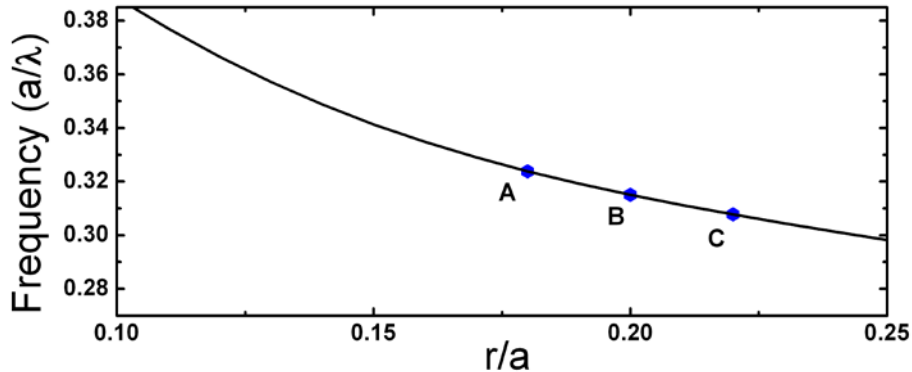


Fig. 3. The relation between the waveguide band cut-off frequency and the dielectric filling factor. The highlighted frequencies correspond to the selected PCW sections.

The dielectric constant of the rods is set to 9.61 in the simulations to achieve a relatively high contrast between the air and the PC structure. The material is chosen as Alumina ( $\text{Al}_2\text{O}_3$ ). The high contrast provides a significant decrease in the cross-talk between the channels as a result of the strong interaction of the slow light modes with the rods. Furthermore, the group velocities of the selected modes are expected to exhibit larger differences if higher dielectric materials are used.

The selection of the operating frequencies in Fig. 4(b) is based on the spatial distributions of the slow light modes inside the PCW sections. Although the lowest group velocity occurs at the band-edge ( $k = 0$ ), the maximum transmission occurs at the wavelengths that are indicated by green dashed lines in Fig. 4(b). This frequency shift can be explained in two ways. Firstly, the modes near  $k = 0$  that are also supported by the main waveguide channel have higher impedances resulting in a high impedance mismatch between the air and the PC structure. Secondly, the maximum of the transmitted intensity does not occur at a mode that has a higher group velocity that is in the linear region of the waveguide mode as a result of the spatial distribution of the modes. Moreover, the optimum spatial fit for the PCW section is related to the length of the section. A longer the PCW section corresponds to a wider spatially distributed slow-light mode which is the optimum fit for the structure. Therefore, there is a linear relation between the PCW length and the width of the spatial distribution, where a wider distribution indicates a slower mode. It can be inferred from the dispersion diagrams that a slower mode occurs at the band-edge. It shows that the length of the PCW and the frequency shift of the peak transmission are inversely proportional. Taking these explanations into account, the operating frequencies are selected by studying the transmission spectra of each PCW section, which is shown in Fig. 5. Moreover, the frequencies that are allowed to propagate through the output channels are limited by the impedance mismatch and the spatial distributions of the modes. Each PCW section operates as a frequency filter and allows only a portion of the modes that are propagating in the main waveguide to propagate. The narrowband transmission can be seen as a coupling mechanism that has a quality factor of nearly 1000. As mentioned in several previous studies, high quality factor values are demanded in frequency division applications [16–18].

The length of the waveguide and the design of the output channels are optimized such that maximum output power is obtained at the operating frequencies. The length of the PCW and the formation of the output channels are optimized in order to achieve the maximum performance. The output channel is a wider waveguide in order to get a gradual group velocity transition between the main and the output waveguides. This gradual transition provides a higher transmission or stronger coupling between the waveguides as a result of the

better match in the impedances. The width of the output waveguides is selected as  $3a$ , which corresponds to a multimode waveguide and creates an easier design. At the utilization of a single-mode but a wider waveguide (compared to a classical photonic crystal waveguide), the improvement of the output power can still be achieved, but further optimizations would be required.

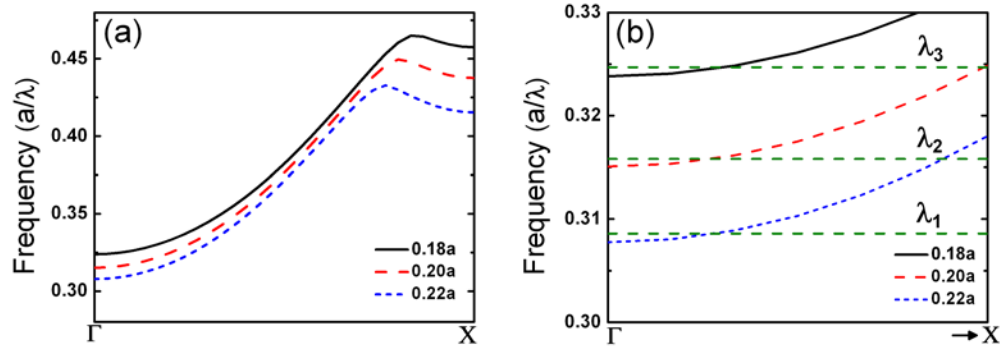


Fig. 4. (a) The evolution of the waveguide bands due to the different dielectric filling factors, (b) the enlarged view of the vicinity of the slow light region, where the dashed lines correspond to the operating frequencies.

The shifts between the de-multiplexed wavelengths are shown in Fig. 5. The  $r/a$  ratios are determined using the evolution of cut-off frequencies that is shown in Fig. 3. We choose the ratios as  $a_1/\lambda_1 = 0.3086$ ,  $a_2/\lambda_2 = 0.3158$ , and  $a_3/\lambda_3 = 0.3247$ . These ratios are created by changing the periodicity of each PCW section and keeping the radii of rods constant. Therefore, each normalized frequency for each PCW section is unique. One can see that, each wavelength is picked up by the relevant output channel. The numerical results are compared to the experimental results for each PCW y that is used in the cascaded PC structure. Alumina rods with a radius of 0.158 cm and a length of 15.32 cm are used in the experiments. Therefore, the periodicities are selected as 0.878 cm, 0.79 cm, 0.718 cm for  $r = 0.18a$ ,  $r = 0.20a$  and  $r = 0.22a$ , respectively. The proposed structure is installed between two platforms that have comparable dielectric constants to that of the free space. The experiments are conducted using two standard horn antennas that are placed 10 cm away from the input and output channels. An HP-8510C network analyzer (Agilent Technologies, USA) is used to measure the transmission coefficients. The frequency shifts between the de-multiplexed waves are observed in the experiments. A slight frequency shift occurred between the numerical and experimental results possibly because of fabrication inconsistencies and impurities in the Alumina rods. The usage of alumina rods can also cause power leakage in the  $z$ -direction. However, the leakage is prevented by using relatively long rods ( $\sim 100r$ ). In Fig. 5, the good agreement between the numerical and experimental results proves that a significant leakage in the  $z$ -direction is not observed. The results of different sections are shown separately because of the method that is used when conducting the experiments that is changing the periodicity which creates a different normalized frequency axis for each PCW section.

The set of wavelengths are subject to a selection criterion as they travel along the PCW. The wavelength dropping occurs from the largest wavelength to the smallest one. Each PCW acts as a filter due to the difference in their filling factors. Assuming that the light has the appropriate wavelength to propagate through the first PCW, the second PCW checks the wavelength and allows the light to pass if the wavelength of light corresponds to a propagating mode, in other words, whether it is distant from the slow light region. Otherwise, the light begins to diffuse sideways through the output channels. Every section of the structure performs a similar task. Briefly, each section either allows the light to pass by or couples the light to the appropriate channel. If none of the PCW sections select the input wavelength, then the light will propagate through the device without any spreading in the transverse direction and reaches the end of the waveguide. The injection ratio between the input waveguide and

the air is lower than that of a wave propagating in the linear regime of the waveguide mode since slow light modes have higher impedances. However, injection ratio can be improved by transferring the input wavelengths from a second waveguide which has the same characteristics with the output channel. This optimization is also used in the improvement of the extraction ratio by using output waveguides that have a width of  $3a$ . Using a wider waveguide results a gradual transition in the impedances of waveguides and therefore, minimizes the impedance mismatch and increases the output power. This can also be seen as an incentive idea to design input or output couplers for photonic crystal based slow light devices. The transmitted power at output channels is smaller than the power at the output of the main waveguide considering the usage of a single PCW section as a de-multiplexer. However, the cascaded design of PCW sections is designed to prevent the propagation of the wavelengths that are already de-multiplexed by adjusting the dielectric filling factors of each PCW section to reflect the wavelengths by using the stop bands of the cascaded waveguides. For the composite structure, the extracted power levels at output channels are much larger than the power levels of the same wavelengths in the main waveguide as a result of the reflection of each de-multiplexed wavelengths at the surface of the next PCW section.

In the simulations, the results for the composite structure are obtained by keeping the periodicity for each PCW section constant and adjusting the radii of rods for each section to keep the  $r/a$  ratios. Figure 6(a) shows the steady-state electric field distribution due to the incident light whose normalized frequency is  $a/\lambda = 0.3086$ . This frequency is within the PBG of the first PCW and below that of the second PCW. It is expected that this frequency is dropped at the first channel. This observation can be confirmed from the FDTD result shown in Fig. 6(a). Similarly, when the normalized input frequency is switched to  $a/\lambda = 0.3158$ , this pulse can propagate without any spreading until the second section of the structure. Afterwards, in the second section, it enters the slow light regime and therefore is picked up from the second channel. Figure 6(b) confirms this wavelength selection rule by presenting the distribution of the steady-state fields. Similarly, Fig. 6(c) shows the selectivity of the wavelength at  $a/\lambda = 0.3247$ . A typical unselected wavelength at  $a/\lambda = 0.34$  is shown in Fig. 6(d), which stays confined until the end of the waveguide. It is observed using these figures that each PCW section filters a different wavelength and directs the selected wavelength toward the appropriate drop channel.

We also calculated the spatial distributions of the output channels in  $x$ -direction in Fig. 7. By applying Fourier transform on the time domain data of the output channels, the spectral content of the selected wavelength in a specific channel is determined. The operating frequencies are selected such that, at these frequencies, the transmitted power is maximized whereas the cross-talk between the channels is minimized. The maximum level of the cross-talk for the first channel is obtained as  $-13.7$  dB. The cross-talks are  $-15.6$  dB and  $-28.7$  dB for the second and third channels, respectively.

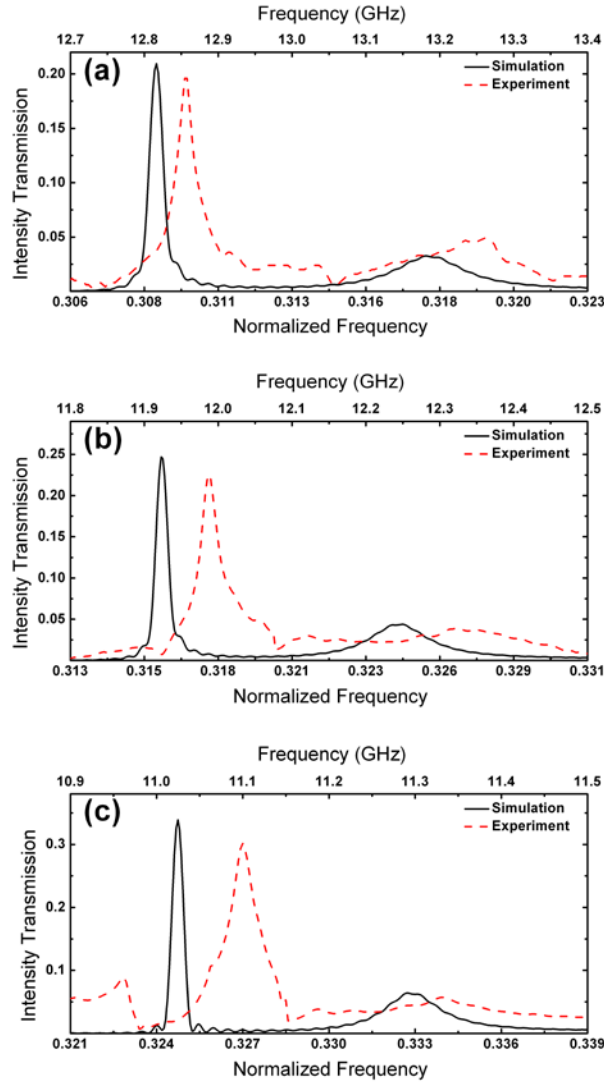


Fig. 5. The output frequency spectra of the channels of each PCW section that has a  $r/a$  ratio of (a) 0.22, (b) 0.2, (c) 0.18, respectively.

The reason of the low cross-talk ratio is the design of the cascaded waveguides that are adjusted to create stop bands for the wavelengths that are already de-multiplexed at the previous channels. Moreover, the transmission spectra of the single PCW sections which are shown in Fig. 5. indicates that the narrowband transmission similar to a resonant structure creates a pass band for only the allowed frequencies and avoids the other frequencies even they are supported in the main waveguide. The noise in the output channels can further be reduced by selecting operating frequencies according to the transmission spectra of the channels. Furthermore, using rods that have higher dielectric constant leads to a stronger separation of selected frequencies as a result of the deeper interaction of the slow light modes with the PC structure. The sinc-like distribution profiles that are obtained in Fig. 7. show that the coupling mechanism between the main waveguide and the output channels successfully works and that the dispersion characteristics of the wavelengths propagating through the main waveguide transform into the dispersion characteristics of the output channels.

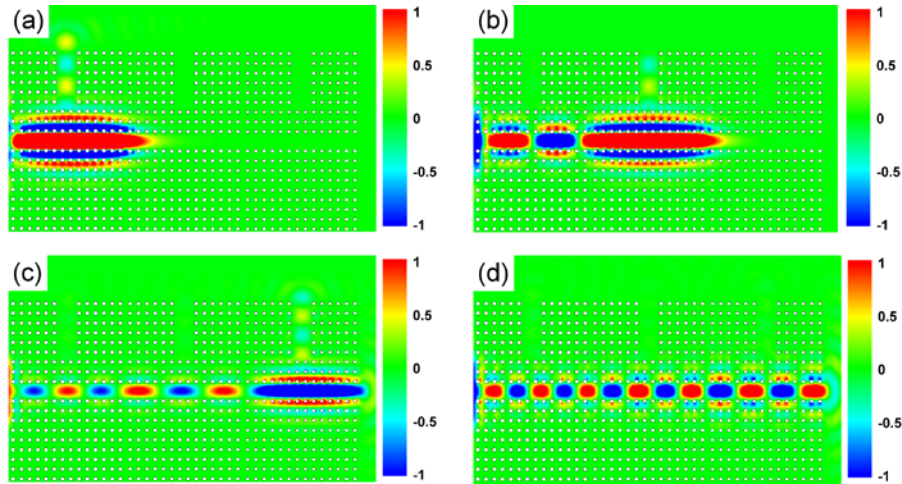


Fig. 6. The steady-state electric field profiles of the three de-multiplexed frequencies for each waveguide channel where the input beam is placed  $5a$  away from the PC structure, (a)  $a/\lambda = 0.3086$ , (b)  $a/\lambda = 0.3158$ , (c)  $a/\lambda = 0.3247$ , (d) the steady-state electric field profile of an unselected frequency, which has a normalized frequency of  $a/\lambda = 0.34$ .

The spectral and spatial shift of the pulses can be obtained clearly by utilizing the presented approach. Further modifications to the geometry may result in changes in the spatial separation, for example, forming a longer PCW section creates a peak transmission frequency which has a smaller group velocity. On the other hand, if the difference of the filling factors between each PCW section is kept smaller, then the spectral selectivity, which is defined as the difference between the de-multiplexed wavelengths, can be increased. In other words, the ability to distinguish between small wavelength shifts can be achieved by introducing small changes in the filling factors. In order to de-multiplex more than three wavelengths, the number of the waveguides, which have different filling factors, needs to be increased. New PCW sections should be designed carefully considering the output power of the single PCW section and the frequency region of the allowed modes in the main waveguide. The new PCW section should also be designed by aiming low cross talk between the channels by creating a stop-band in the vicinity of the wavelengths that are already de-multiplexed in the previous channels.

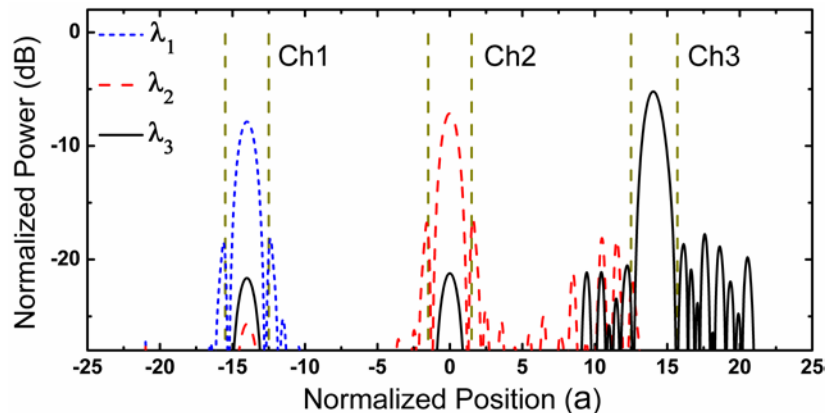


Fig. 7. The spatial distributions of the operating frequencies at three output channels in  $x$ -direction. The output levels are calculated nearly  $5a$  away from the output channels. The green dashed lines show the positions of the output channels in  $x$ -direction.

The usage of PCWs of equal lengths leads to a compact design, although the management of cross-talk between channels becomes more difficult as a consequence of the absence of the minimization of back reflections from each section.

### **3. Conclusion**

In conclusion, we propose a wavelength de-multiplexer design based on concatenated photonic crystal waveguides, for which dielectric filling factors are varied in order to target the slow light region. The frequency selectivity of the device originates from the light behavior in the vicinity of the slow light regime due to the high leakage as a result of the wider spatial distribution of the electromagnetic waves inside the main waveguide. The spatial selection of different wavelengths occurs within consecutive PCW sections and we numerically and experimentally demonstrate the successful de-multiplexing of three wavelengths in a compact manner.

The preliminary results of the DEMUX design employing the slow light phenomena are encouraging. However, the DEMUX design can be further studied in order to obtain higher output power levels at each output channel and a linear spacing in de-multiplexed frequencies. Moreover, using the proposed de-multiplexer design idea, slab dielectric PC structures with air holes in triangular lattice form can be a good candidate to create similar devices that work at optical frequencies avoiding the power leakage in the  $z$ -direction. In addition, the length of each PCW can be optimized to create a more compact design. Such investigations will be the subject of a future study.

### **Acknowledgments**

This work is supported by the European Union (EU) under the projects PHOME, ECONAM, and N4E; by The Scientific and Technological Research Council of Turkey (TUBITAK) under the projects 110T306, 109E301, 107A004, and 107A012; and the State Planning Organization (DPT) under the project DPT-HAMIT. H. Kurt acknowledges support from the Turkish Academy of Sciences Distinguished Young Scientist Award (TUBA GEBIP). One of the authors (E. Ozbay) also acknowledges partial support from the Turkish Academy of Sciences.